Improved BP network based sliding model tracking control for a quadrotor UAV

Qiang-wei Pang, De-shi Wang, Wei Wu, Ye Chen, Yong-yong Zhu

College of Weapon Engineering, Naval University of Engineering, Wuhan 430000, PR China
(e-mail: pqw_aeu@163.com, wdeshi@sina.com, wkw_wuwei@126.com), cy1980sjz@sina.com, zyy99515@126.com)

Abstract: This paper introduced a novel method for trajectory tracking control of a quadrotor UAV under the parametric uncertainties. In order to improve its stability during trajectory tracking, the proposed method combines the advantages of back propagation (BP) network and sliding model control (SMC). Firstly, the expected roll angle and the expected pitch angle are decoupled by the nonlinear dynamic model of quadrotor and the known desired state. Secondly, a sliding model four-channel control law is designed for the nonlinear dynamics model of quadrotor, and the stability of the designed control law is proved by the Lyapunov theorem. Finally, the designed sliding manifold coefficients are solved by the improved BP network. In the Matlab/Simulink environment, compared with other algorithms, the proposed method can accurately track the desired trajectory, effectively compensate the parameters uncertainty, and greatly suppress the chattering phenomenon with the maximum overshoot of the SMC.

Keywords: Quadrotor UAV; Sliding Model control; Improved Back Propagation Algorithm; Tracking control; Chattering phenomenon.

1. INTRODUCTION

More recently, UAV has been one of the research hotpots in the fields of the civil and military applications, such as search and rescue, forest fire prevention, mapping, power plants inspection, reconnaissance, surveillance (ALVEAR O et al., 2018; Kaifang W et al., 2020; M. Hassanalian et al., 2017; Manyam S G et al., 2017; Petr S et al., 2018), etc. UAVs have received extensive attention from many scholars.

When quadrotor UAV are performing military reconnaissance and rescue missions, they usually rely on accurate path planning and robust navigation and attitude controllers. However, the quadrotor UAV is an omnidirectional maneuverable aircraft with four inputs and six degrees of freedom, which is under-actuated, strongly coupled and vertical takeoff and landing. Therefore, it has always been a difficult and key point to design an accurate and reasonable attitude controller to control the stability of the quadrotor UAV to ensure the smooth execution of the mission.

At present, various trajectory tracking control methods have been rushed to be studied and applied by scholars. Such as nonlinear PID control (J. Moreno-Valenzuela et al., 2018), nonlinear adaptive control technology (R.C. Avram et al., 2017), model predictive control (G. Cao et al., 2017), LQR control method (M. Faessler et al., 2017), robust linear parameter change observer LPV (F.R. Lopez-Estrada et al., 2016), sliding model control SMC (H. Casta et al., 2019; Khebbache, H. et al., 2013). The more effective method is SMC, because it has good instantaneous performance, easy operation, and can compensate the parameters uncertainty with strong anti-interference ability (A. Zulu et al., 2014).

In order to compensate the uncertainty of parameters, an adaptive SMC method is introduced in (O. Mofid et al., 2018) for the stability control of UAV. In (Y. Yang et al., 2016), the fuzzy logic is used to solve the parameters of the adaptive sliding manifold, so as to realize the attitude control of the quadrotor UAV. In (Zheng et al., 2014), a second-order SMC (2-SMC) is proposed for position and attitude tracking of quadrotor UAV. In (XIONG et al., 2016), the quadrotor dynamic model is divided into a fully-actuated subsystem and an under-actuated subsystem, then a fast terminal SMC method is proposed for attitude control. In (M. Labbadi et al., 2019), a nonlinear control strategy that combining the back-stepping method with fast terminal SMC is proposed to track the trajectory of the quadrotor UAV. In order to suppress the chattering phenomenon, in (Z. Jia et al., 2017), a method that combines the integral method with the SMC is proposed, which effectively avoids the chattering phenomenon caused by the conventional control. In (Hadi R, 2018), the combination of neural network and SMC is used to control the quadrotor. However, the vibration of the designed controller was relatively large, which resulted in a large maximum overshoot in the whole tracking process. On this basis, a neural network-based adaptive SMC was suggested in (Hadi R et al., 2019) to control the attitude of the quadrotor UAV, but there are still more chattering phenomena.

All the above methods can effectively track the expected trajectory and suppress the chattering phenomenon by compensating the parameter uncertainty of the quadrotor UAV. However, in practical application, there are still the following shortcomings:

• Most scholars assumed that the expected roll angle and the expected pitch angle are 0, which will lead to over-compensation for parameter uncertainty and then cause chattering when designing the controller.

• During the continuous time-varying switching of the control signal, the high frequency chattering of the controller is caused by the fixity of individual parameters.

• The maximum overshoot is relatively large during the chattering process.

• The designed controller is more complicated, which makes its stability difficult to analyze.

At present, the BP network as a forward neural network algorithm, its weight can be adjusted by backpropagation to realize arbitrary non-linear mapping from input to output (WU B et al., 2016). Therefore, this paper expects to use the BP network to accurately approximate the nonlinearity of the quadrotor UAV, so as to achieve the objective of stably controlling the quadrotor UAV.

Therefore, in order to accurately compensate for the parameters uncertainty of the quadrotor UAV and suppress its chattering phenomenon during the design of the trajectory tracking controller, meanwhile expand the application range of neural network, the improved BP network based sliding model tracking control for a quadrotor UAV is proposed by draws on the advantages of SMC and BP networks. Firstly, the nonlinear dynamics model of the quadrotor UAV is built by using Newton-Euler equation. Secondly, on the basis of the dynamic model of the quadrotor UAV and desired state, the expected roll angle and the expected pitch angle are first decoupled. And the entire control system is divided into a fully-actuated subsystem and an under-actuated subsystem, then through SMC to design the controller for each subsystem, and Lyapunov stability theory is used to prove the stability of the designed control law. Finally, on the basis of the idea of adjusting the weight of the steepest descent gradient of the BP network, the variable learning rate momentum BP network is used to solve the controller parameters. The simulation results verify the effectiveness of the proposed method. Compared with the 2-SMC and standard BP network, it effectively suppresses the chattering phenomenon and the maximum overshoot of the SMC, and the desired trajectory can be accurately tracked.

The remaining part of the paper is structured as follows. In the second section, the nonlinear dynamics equation of the quadrotor UAV is established according to the Newton-Euler equation. In the third section, the controller is designed based on SMC. In the fourth section, the controller parameters are solved based on the improved BP network. In the fifth section, the simulation and comparison results are shown. Finally, the conclusion is given in Section 6.

2. QUADROTOR DYNAMICAL MODEL

The quadrotor is a highly coupled under-actuated system, as shown in Fig. 1, it contains four motors, which control the rotation speed of the four motors to generate lift and torque to control a series of movements of the UAV, such as lifting, forward and backward, left and right, pitching, rolling, yawing and so on.

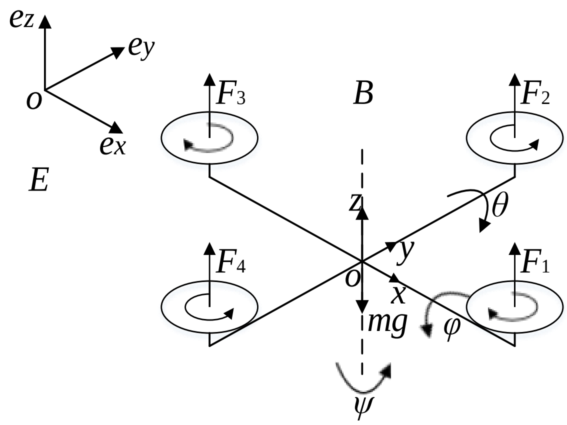

Fig. 1. Structure diagram of Quadrotor UAV

Several assumptions are made in order to facilitate the establishment of the quadrotor's dynamical model. The assumptions are as:

Assumption 1. The quadrotor UAV is a rigid symmetrical structure;

Assumption 2. The center of mass of the quadrotor UAV coincides with the origin of the body's coordinates;

Assuming that the position of the quadrotor in the earth-frame is P=$[x, y, z]$, and the attitude in the body-frame is $\eta = [\phi, \theta, \psi]$, according to the Newton-Euler equation, the dynamic equation of the quadrotor is:

$$\begin{cases} F R_B^E = m\ddot{P} - m g_z \\ M = J\ddot{\eta} + \dot{\eta} \times J\dot{\eta} \end{cases} \tag{1}$$

Where, F denotes the total lift force generated by the four motors; R_B^E denotes the rotation matrix from the body-frame to the earth-frame; m denotes the mass of the quadrotor; g_Z denotes the accelerant of gravity; M denotes the torque generated by the four motors; J denotes the inertia matrix $diag[I_x, I_y, I_z]$.

Assuming that the input generated by the four motors is U_1, U_2, U_3, U_4, then the dynamics model of the quadrotor UAV can be describe by the following equations:

$$\begin{cases} \ddot{x} = \dfrac{U_1}{m}(\sin\psi\sin\varphi + \cos\psi\sin\theta\cos\varphi) \\ \ddot{y} = \dfrac{U_1}{m}(-\cos\psi\sin\varphi + \sin\psi\sin\theta\cos\varphi) \\ \ddot{z} = \dfrac{U_1}{m}\cos\theta\cos\varphi - g \\ \ddot{\varphi} = \dfrac{I_y - I_z}{I_x}\dot{\theta}\dot{\psi} + \dfrac{l}{I_x}U_2 \\ \ddot{\theta} = \dfrac{I_z - I_x}{I_y}\dot{\varphi}\dot{\psi} + \dfrac{l}{I_y}U_3 \\ \ddot{\psi} = \dfrac{I_x - I_y}{I_z}\dot{\varphi}\dot{\theta} + \dfrac{d}{I_z}U_4 \end{cases} \tag{2}$$

Where, l represents the distance from the center of each rotor to the center of gravity; d and k are the parameters of the motor and propeller. φ and θ are roll angle and pitch angle, the value range is (-π/2, π/2). ψ is yaw angle, the value range is (-π, π).

$$\begin{bmatrix} U_1 \\ U_2 \\ U_3 \\ U_4 \end{bmatrix} = \begin{bmatrix} 1 & 1 & 1 & 1 \\ l & 0 & -l & 0 \\ 0 & l & 0 & -l \\ -k & k & -k & k \end{bmatrix} \begin{bmatrix} F_1 \\ F_2 \\ F_3 \\ F_4 \end{bmatrix} \tag{3}$$

Where, F_1, F_2, F_3, F_4 is the lift force generated by the four motors respectively.

3. CONTROLLER DESIGN

For equation (2), it can be rewritten as a state-space equation:

$$\begin{bmatrix} \ddot{z} \\ \ddot{\psi} \end{bmatrix} = \begin{bmatrix} \dfrac{\cos\theta\cos\varphi}{m} \\ \dfrac{d}{I_z} \end{bmatrix} \begin{bmatrix} U_1 \\ U_4 \end{bmatrix} + \begin{bmatrix} -g \\ \dfrac{I_x - I_y}{I_z}\dot{\varphi}\dot{\theta} \end{bmatrix} \tag{4}$$

$$\begin{cases} \begin{bmatrix} \ddot{x} \\ \ddot{y} \end{bmatrix} = \begin{bmatrix} \cos\psi & \sin\psi \\ \sin\psi & -\cos\psi \end{bmatrix} \begin{bmatrix} \cos\varphi\sin\theta \\ \sin\varphi \end{bmatrix} \dfrac{U_1}{m} \\ \begin{bmatrix} \ddot{\varphi} \\ \ddot{\theta} \end{bmatrix} = \begin{bmatrix} \dfrac{l}{I_x} & 0 \\ 0 & \dfrac{l}{I_y} \end{bmatrix} \begin{bmatrix} U_2 \\ U_3 \end{bmatrix} + \begin{bmatrix} \dfrac{I_y - I_z}{I_x}\dot{\theta}\dot{\psi} \\ \dfrac{I_z - I_x}{I_y}\dot{\psi}\dot{\varphi} \end{bmatrix} \end{cases} \tag{5}$$

From the above state-space equation, we can see that the whole quadrotor control system can be divided into fully-actuated subsystem and under-actuated subsystem. The design block diagram of the whole quadrotor controller is shown in Fig. 2.

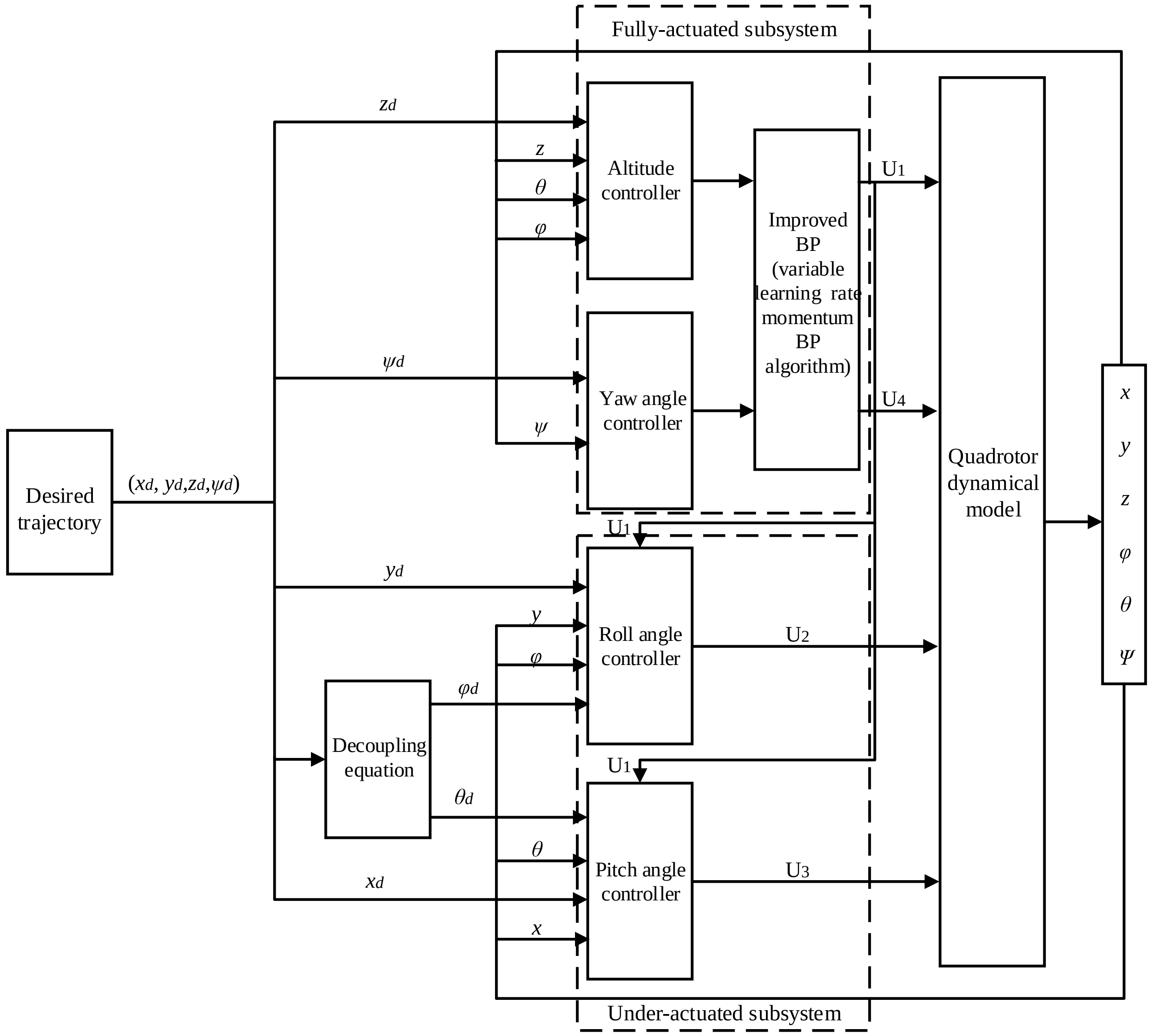

Fig.2. Block diagram of the quadrotor UAV controller design

3.1 Expected Euler angle

When designing quadrotor trajectory tracking control, most scholars assumed that the expected roll angle and the expected pitch angle are 0. However, after the expected state is given, due to the highly coupling of quadrotor UAV, its corresponding expected roll angle and expected pitch angle is also given. So the common method in the controller design will cause over-compensation for parameter uncertainty, which will cause chattering phenomenon.

Therefore, in order to minimize the over-compensation caused by ignoring the expected roll angle and expected pitch angle in the under-actuated (roll and pitch) controller design. By inverse solution of differential equation (2), the decoupling calculation formula of expected roll angle φ_d and expected pitch angle θ_d can be obtained as follows:

$$\begin{cases} \tan\varphi_d = \dfrac{\cos\theta_d\,(\ddot{x}_d\sin\psi_d - \ddot{y}_d\cos\psi_d)}{\ddot{z}_d + g} \\ \varphi_d = \arctan\left(\dfrac{\cos\theta_d\,(\ddot{x}_d\sin\psi_d - \ddot{y}_d\cos\psi_d)}{\ddot{z}_d + g}\right) \end{cases} \tag{6}$$

$$\begin{cases} \tan\theta_d = \dfrac{\ddot{x}_d\cos\psi_d + \ddot{y}_d\sin\psi_d}{\ddot{z}_d + g} \\ \theta_d = \arctan\left(\dfrac{\ddot{x}_d\cos\psi_d + \ddot{y}_d\sin\psi_d}{\ddot{z}_d + g}\right) \end{cases} \tag{7}$$

Then expected roll angle and expected pitch angle are used for tracking design, which can effectively reduce chatter caused by frequent corrections due to over-compensation.

3.2 Fully-actuated controller design

In order to ensure that under the control of U_1 and U_4 within a finite time, the state variable height z and yaw angle ψ can converge to the desired value z_d and ψ_d, and the error of height is taken as $e_z = z_d - z$, the yaw error is $e_\psi = \psi_d - \psi$, then the sliding manifolds are defined as

$$\begin{cases} s_z = c_z e_z + \dot{e}_z \\ s_\psi = c_\psi e_\psi + \dot{e}_\psi \end{cases} \tag{8}$$

Where, c_z and c_ψ are the design parameters to be solved.

3.3 Under-actuated controller design

In order to ensure that under the coupled control of U_2 with U_3 and U_1 in a finite time, the corresponding state variables x and θ converge to the expected value x_d and θ_d, and y with φ converge to the desired value y_d and φ_d, the corresponding error are taken as $e_x = x_d - x$, $e_\theta = \theta_d - \theta$, $e_y = y_d - y$, $e_\varphi = \varphi_d - \varphi$, the sliding manifolds are defined as

$$\begin{cases} s_\varphi = c_1 e_y + c_2\dot{e}_y + c_3 e_\varphi + c_4\dot{e}_\varphi \\ s_\theta = c_5 e_x + c_6\dot{e}_x + c_7 e_\theta + c_8\dot{e}_\theta \end{cases} \tag{9}$$

Where, $c_i(i = 1,\cdots,8)$ is sliding manifold coefficient, this paper obtains directly from the method of (Zheng et al., 2014),

$$\begin{cases} c_1 = -\dfrac{6m}{U_1\cos\psi} \\ c_2 = -\dfrac{11m}{U_1\cos\psi} \\ c_3 = c_7 = 6 \\ c_4 = c_8 = 1 \\ c_5 = \dfrac{6m}{U_1\cos\varphi\cos\psi} \\ c_6 = \dfrac{11m}{U_1\cos\varphi\cos\psi} \end{cases} \tag{10}$$

Take the approach rate $\dot{s}_i = -\varepsilon_i\tanh(s_i) - \beta_i s_i$, where is ε_i the design parameter and β_i is the positive constant. Since the quadrotor is a rigid body and symmetrical, then $I_x = I_y$, substituting equations (8) and (9) into the approach rate, the corresponding four control inputs can be obtained as:

$$\begin{cases} U_1 = \dfrac{m\{c_z\dot{e}_z + \ddot{z}_d + g + \varepsilon_z\tanh(s_z) + \beta_z s_z\}}{\cos\theta\cos\phi} \\ U_2 = \dfrac{I_x}{lc_4}\{c_1\dot{e}_y + c_2\ddot{e}_y + c_3\dot{e}_\varphi + \ddot{\varphi}_d + \varepsilon_\varphi\tanh(s_\varphi) \\ \qquad -\dfrac{1}{I_x}(I_y - I_z)\dot{\theta}\dot{\varphi} + \beta_\varphi s_\varphi\} \\ U_3 = \dfrac{I_y}{lc_8}\{c_5\dot{e}_x + c_6\ddot{e}_x + c_7\dot{e}_\theta + \ddot{\theta}_d + \varepsilon_\theta\tanh(s_\theta) \\ \qquad -\dfrac{1}{I_y}(I_z - I_x)\dot{\varphi}\dot{\psi} + \beta_\theta s_\theta\} \\ U_4 = \dfrac{I_z}{d}\{c_\psi\dot{e}_\psi + \ddot{\psi}_d + \varepsilon_\psi\tanh(s_\psi) + \beta_\psi s_\psi\} \end{cases} \tag{11}$$

3.4 Stability analysis

The Lyapunov function is constructed as:

$$V = \frac{{s_i}^2}{2} \tag{12}$$

then

$$\begin{aligned} \dot{V} &= s_i\dot{s}_i = s_i(-\varepsilon_i\tanh(s_i) - \beta_i s_i) \\ &\le -\varepsilon_i|s_i| - \beta_i {s_i}^2 \le 0 \end{aligned} \tag{13}$$

According to Lyapunov stability theorem, the control system is asymptotically stable. Therefore, under the control of the designed control law, the quadrotor UAV can converge to the expected state within a finite time.

4. IMPROVED BP NETWORK”

BP network is a forward neural network algorithm that can adjust its weights through backpropagation, and has good fault tolerance (Alejandro G-G et al., 2020). Therefore, in order to enhance accuracy of the neural network algorithm, and suppress the high frequency chatter caused by the continuous time-varying switching of the control signal due to the fixity of individual parameters. An improved BP network is adopted to solve the parameters of the fully-actuated sliding manifolds based on the idea of weight correction of the neural network.

4.1 Standard BP network

Fig. 3 shows the height control based on the standard BP network, where$e_z = z_d - z$, the height z is adjusted to make the tracking error e_z approach 0 under the control of the structure, and then the height tracking control is performed.

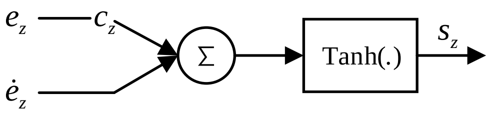

Fig.3. Block of sliding manifold calculating based on standard BP network

In order to make the error as small as possible, let

$$E_z = \frac{1}{2} {e_z}^2 = \frac{1}{2}(z_d - z)^2 \tag{14}$$

According to the steepest gradient descent method, we can get:

$$\begin{cases} \varepsilon_{z,k+1} = \varepsilon_{z,k} - \alpha_z \dfrac{\partial E_{z,k}}{\partial \varepsilon_{z,k}} \\ c_{z,k+1} = c_{z,k} - \alpha_z \dfrac{\partial E_{z,k}}{\partial c_{z,k}} \end{cases} \tag{15}$$

Where, α_z is the learning rate, $\partial E_{z,k}/\partial \varepsilon_{z,k}$ and $\partial E_{z,k}/\partial c_{z,k}$ is the gradient vector of the output error to ε_z and c_z when the neural network iterates to the k-th time, then

$$\frac{\partial E_{z,k}}{\partial \varepsilon_{z,k}} = \frac{\partial E_{z,k}}{\partial z}\frac{\partial z}{\partial U_1}\frac{\partial U_1}{\partial \varepsilon_{z,k}} = -\frac{m e_z \tanh(s_z)}{\cos\theta\cos\varphi}\frac{\partial z}{\partial U_1} \tag{16}$$

$$\begin{aligned} \frac{\partial E_{z,k}}{\partial c_{z,k}} &= \frac{\partial E_{z,k}}{\partial z}\frac{\partial z}{\partial U_1}\frac{\partial U_1}{\partial s_z}\frac{\partial s_z}{\partial c_{z,k}} = -e_z \frac{\partial z}{\partial U_1}\frac{\partial U_1}{\partial s_z} e_z \\ &= -\frac{m\left[\dfrac{\varepsilon_z 4e^{-2s_z}}{(1+e^{-2s_z})^2} + \beta_z\right]{e_z}^2}{\cos\theta\cos\varphi}\frac{\partial z}{\partial U_1} \end{aligned} \tag{17}$$

4.2 Variable learning rate momentum BP network

Due to the invariance of the learning rate of the standard BP network, the controller will oscillate more frequently. This is because when the learning rate is bigger, as the tracking effect of the controller gets closer and closer to the desired state, it will cause a large overshoot at each step which will cause the controller to oscillate back and forth. When the learning rate is lesser, it will accumulate a small amount of momentum energy, and fall into the local optimum, and cannot jump out of the local optimum in time.

In order to enhance its stability and reduce its oscillation, it is necessary to make the learning rate as large as possible at the beginning, and then the learning rate gradually changes along the stable direction, that is, the step size can be dynamically adjusted. Therefore, the variable learning rate factor is introduced. When the error tends to 0 in a decreasing way, it indicates that the correction direction is correct and the step size can be increased. the learning rate is multiplied by the incremental factor $k_{inc}(1 < k_{inc})$. When the error becomes larger and larger, it indicates that the correction is excessive and the step size should be reduced, the learning rate is multiplied by the decrement factor $k_{dec}(0 < k_{dec} < 1)$, that is

$$\alpha_{z,k+1} = \begin{cases} k_{inc}\alpha_{z,k} & E_{z,k+1} \le E_{z,k} \\ k_{dec}\alpha_{z,k} & E_{z,k+1} > E_{z,k} \end{cases} \tag{18}$$

On the basis of the fastest gradient descent algorithm, the momentum factor η is introduced, and the parameter adjustment operator is obtained

$$\Delta\varepsilon_{z,k+1} = \eta\varepsilon_{z,k} + \alpha_{z,k}(1-\eta)\frac{\partial E_{z,k}}{\partial \varepsilon_{z,k}} \tag{19}$$

$$\Delta\varepsilon_{z,k+1} = \eta\varepsilon_{z,k} + \alpha_{z,k}(1-\eta)\frac{\partial E_{z,k}}{\partial \varepsilon_{z,k}} \tag{20}$$

This operator is the result of the previous correction to adjust the current correction. When the previous correction amount is excessive, the sign of the two terms of the adjustment operator will be opposite $(\eta \ge 1, E_{z,k-1} \ge E_z)$, so that the current correction amount will be reduced and the oscillation will be suppressed. When the previous correction amount is insufficient, the sign of the two terms of the adjustment operator will be the same $(0 < \eta < 1, E_{z,k} > E_{z,k-1})$, so that the current correction amount will be increased, which accelerate the correction effect. The introduction of momentum factor will not cause the divergence of the learning process, because when the correction is excessive or insufficient, the operator will be corrected in time so that the correction direction is towards the direction of convergence.

As time goes on, the indicators of the designed controller is gradually tending to be stable. Because of $\frac{\partial z}{\partial U_1} = \frac{\partial z}{\partial t}\frac{\partial t}{\partial U_1} = \frac{\dot{z}}{\dot{U}_1}$, the change of $\dot{U}_1$ gradually tends to zero, which may lead to the controller designed in the result of a limited period of time is infinite. That is a singular point, which causes the entire controller start from this point is not stable. Therefore, assuming $\frac{\partial z}{\partial U_1}$=$sign(\frac{\partial z}{\partial U_1})$ and sorting out the above content, the correction formulas for ε_z and c_z can be obtained as

$$\begin{aligned} \varepsilon_{z,k+1} &= \varepsilon_{z,k} + \Delta\varepsilon_{z,k+1} \\ &= \varepsilon_{z,k} + \eta\varepsilon_{z,k} + \alpha_{z,k}(1-\eta)\frac{\partial E_{z,k}}{\partial \varepsilon_{z,k}} \\ &= (1+\eta)\varepsilon_{z,k} - \frac{m\alpha_{z,k}(1-\eta)}{\cos\theta\cos\varphi} sign\left(\frac{\partial z}{\partial U_1}\right) \\ &\quad \tanh(s_z) e_z \end{aligned} \tag{21}$$

$$\begin{aligned} c_{z,k+1} &= c_{z,k} + \Delta c_{z,k+1} \\ &= c_{z,k} + \eta c_{z,k} + \alpha_{z,k}(1-\eta)\frac{\partial E_{z,k}}{\partial c_{z,k}} \\ &= (1+\eta)c_{z,k} - \frac{m\alpha_{z,k}(1-\eta)}{\cos\theta\cos\varphi} sign\left(\frac{\partial z}{\partial U_1}\right) \\ &\quad \left[\frac{\varepsilon_z 4e^{-2s_z}}{(1+e^{-2s_z})^2} + \beta_z\right]{e_z}^2 \end{aligned} \tag{22}$$

Likewise, the Variable learning rate momentum BP network is used to adjust the gradient vector of the output error to ε_ψ and c_ψ when the neural network iterates to the k-th time:

$$\frac{\partial E_{\psi,k}}{\partial \varepsilon_{\psi,k}} = \frac{\partial E_{\psi,k}}{\partial \psi}\frac{\partial \psi}{\partial U_4}\frac{\partial U_4}{\partial \varepsilon_{\psi,k}} = -e_{\psi}\frac{\partial \psi}{\partial U_4}\frac{I_z}{d}\tanh\left(s_{\psi}\right) = -\frac{I_z e_{\psi}\tanh\left(s_{\psi}\right)}{d} sign\left(\frac{\partial \psi}{\partial U_4}\right) \tag{23}$$

$$\frac{\partial E_{\psi,k}}{\partial c_{\psi,k}} = \frac{\partial E_{\psi,k}}{\partial \psi}\frac{\partial \psi}{\partial U_4}\frac{\partial U_4}{\partial s_{\psi}}\frac{\partial s_{\psi}}{\partial c_{\psi,k}} = -e_{\psi}\frac{\partial \psi}{\partial U_4}\frac{\partial U_4}{\partial s_{\psi}} e_{\psi} = -e_{\psi}{}^{2}\frac{I_z}{d}\left[\frac{\varepsilon_{\psi}4e^{-2s_{\psi}}}{\left(1+e^{-2s_{\psi}}\right)^2}+\beta_{\psi}\right] sign\left(\frac{\partial \psi}{\partial U_4}\right) \tag{24}$$

The coefficients ε_{ψ} and ε_{ψ}, and following results are obtained:

$$\begin{aligned}\varepsilon_{\psi,k+1} &= \varepsilon_{\psi,k} + \Delta\varepsilon_{\psi,k+1} \\ &= \varepsilon_{\psi,k} + \eta\varepsilon_{\psi,k} + \alpha_{\psi,k}(1-\eta)\frac{\partial E_{\psi,k}}{\partial \varepsilon_{\psi,k}} \\ &= (1+\eta)\varepsilon_{\psi,k} - \alpha_{\psi,k}(1-\eta)\frac{I_z}{d} sign\left(\frac{\partial \psi}{\partial U_4}\right) \tanh\left(s_{\psi}\right) e_{\psi}\end{aligned} \tag{25}$$

$$\begin{aligned}c_{\psi,k+1} &= c_{\psi,k} + \Delta c_{\psi,k+1} \\ &= c_{\psi,k} + \eta c_{\psi,k} + \alpha_{\psi,k}(1-\eta)\frac{\partial E_{\psi,k}}{\partial c_{\psi,k}} \\ &= (1+\eta)c_{\psi,k} - \alpha_{\psi,k}(1-\eta)\frac{I_z}{d} sign\left(\frac{\partial \psi}{\partial U_4}\right) \left[\frac{\varepsilon_{\psi}4e^{-2s_{\psi}}}{\left(1+e^{-2s_{\psi}}\right)^2}+\beta_{\psi}\right] e_{\psi}{}^{2}\end{aligned} \tag{26}$$

5. SIMULATION RESULT AND ANALYSIS

In the section, the performance of the proposed method in the presence of parametric uncertainties by simulation in the MATLAB/Simulink R2020b (64 bit) software, which is equipped with a workstation consisting of AMD Ryzen 9 3900XT 12-Core Processor, 32GB, 64-bit Win7 operating system. Moreover, the advantage of the proposed control method is highlighted through the comparison with 2-SMC and standard BP network.

The quadrotor's parameters are shown in Table 1.

Table 1. Quadrotor parameters.

Parameter	Value
m(kg)	1.1
l(m)	0.21
I_x($\mathrm{N \cdot s^2 \cdot rad^{-1}}$)	1.22
I_y($\mathrm{N \cdot s^2 \cdot rad^{-1}}$)	1.22
I_z($\mathrm{N \cdot s^2 \cdot rad^{-1}}$)	2.2
g($\mathrm{m \cdot s^{-2}}$)	9.8
k($\mathrm{N/ms^2}$)	2
d	1

Moreover, the proposed controller parameters are given in Table 2.

Table 2. Controller parameters.

Parameter	Value
$\alpha_{z,0}$	0.01
$\alpha_{\psi,0}$	0.1
$c_{z,0}$	0.1
$c_{\psi,0}$	0.1
$\varepsilon_{z,0}$	0.1
$\varepsilon_{\psi,0}$	0.1
β_z	0.3
β_{ψ}	2
η	1.5 or 0.5
c_1	$-6m/(U_1\cos\psi)$
c_2	$-11m/(U_1\cos\psi)$
c_3	6
c_4	1
c_5	$6m/(U_1\cos\psi\cos\varphi)$
c_6	$11m/(U_1\cos\psi\cos\varphi)$
c_7	6
c_8	1
β_{θ}	5
β_{φ}	5
ε_{θ}	0.5
ε_{φ}	0.5
k_{inc}	1.1
k_{dec}	0.9

The starting position of the quadrotor UAV is (0,0,0) m and the initial Euler angle is (0,0,0) rad, and the desired 3D tracking trajectory are shown in Table 3:

Table 3. The desired 3D tracking trajectory

Parameter	10 s	20 s	30 s	40 s	50 s
$x_d(m)$	0.3	0.3	0.3	0.6	0.6
$y_d(m)$	0.6	0.3	0.3	0.3	0.6
$z_d(m)$	0.6	0.6	0.6	0.6	0.6
$\psi_d(rad)$	0.5	0.5	0.5	0.5	0.5

In order to show the effectiveness of the proposed method, it will be compared with the standard BP network and 2-SMC.

As shown in Fig. 4, it is the simulation result of the quadrotor UAV tracking the expected trajectory under the control of three methods.

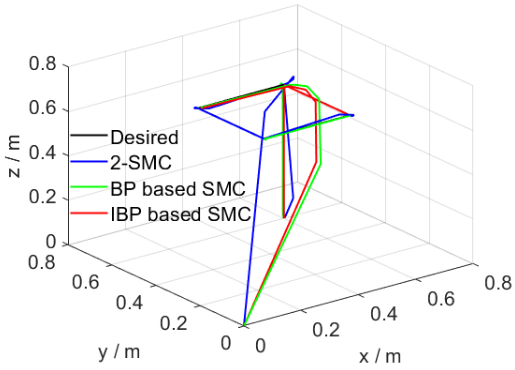

Fig.4. Quadrotor's path

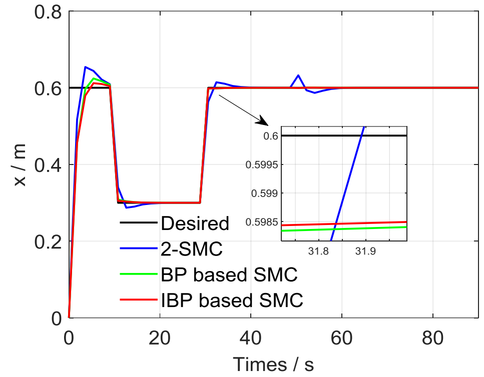

(a)

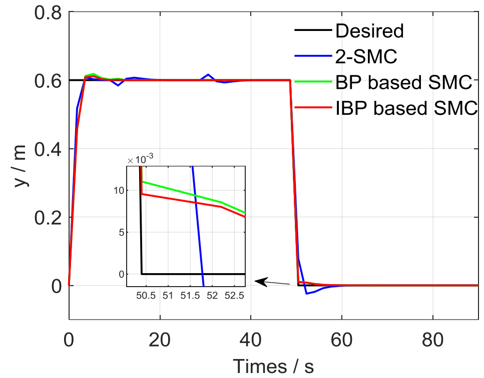

(b)

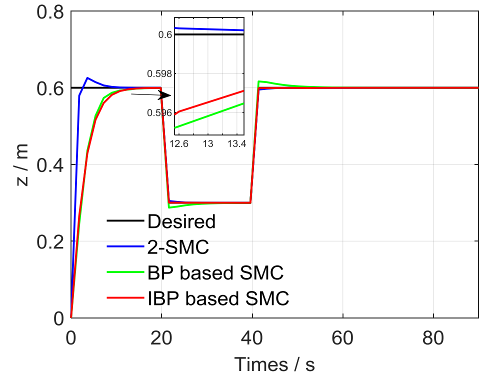

(c)

Fig.5. Position tracking result

Fig. 5 shows the simulation results of the quadrotor UAV tracking the expected position x_d (a), y_d (b) and z_d (c) respectively under the control of the three methods. It can be seen from the figure that when the proposed method tracks the desired position, compared with the other two methods, it is obvious that the chattering phenomenon and the maximum overshoot are greatly reduced. Compared with the standard BP network, the tracking accuracy of the proposed method is higher.

Fig. 6 shows the simulation results of the quadrotor UAV tracking the desired attitude φ_d, θ_d and ψ_d under the control of three methods. It can be seen from the figure (a), (c), (e) that when the quadrotor UAV tracks the desired pitch and the desired roll angles, the actual pitch and roll angles under the control of the proposed method are greater than under the control of the other two methods. This is because this paper first decouples the expected pitch angle and the expected roll angle according to the desired trajectory, and then tracks them in the design controller. The other two methods are designed by assuming that the expected pitch angle and the expected roll angle are zero. Therefore, even under the same parameter uncertainty compensation, the angle of the method in this paper is naturally larger. Analysis of the comparison chart (b, d & f) of the error results shows that the angle compensation required under the proposed method is much smaller than that required by the other two methods, and the chatter phenomenon is significantly reduced. This shows that under the control of the proposed method, only a small correction is needed to make the quadrotor UAV accurately track the expected attitude, thereby enhancing the stability of the attitude tracking.

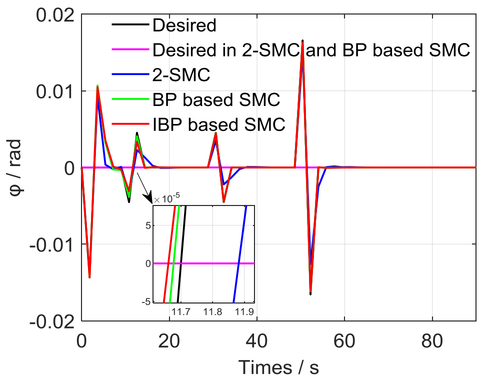

(a)

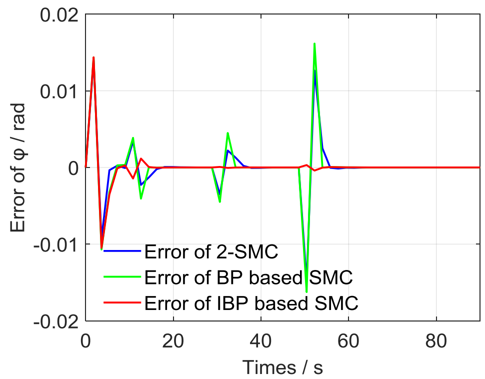

(b)

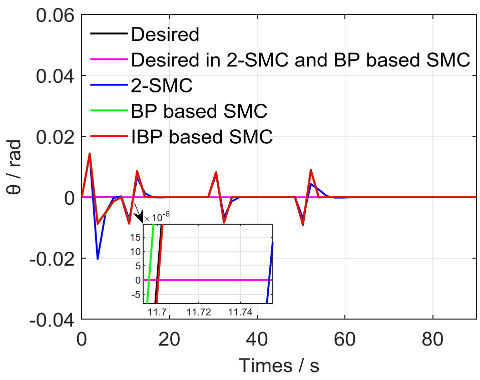

(c)

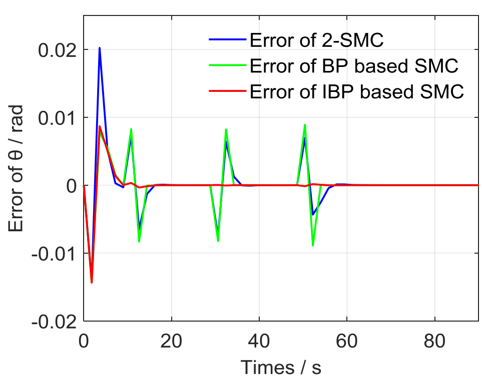

(d)

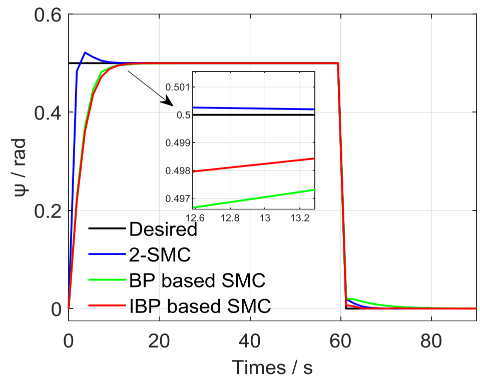

(e)

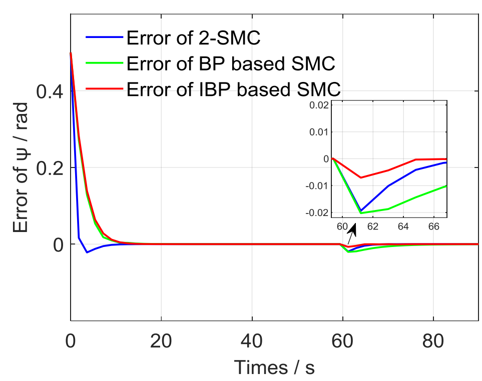

(f)

Fig.6. Attitude tracking results and error results

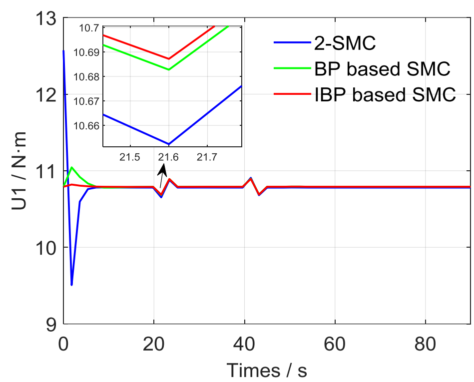

(a)

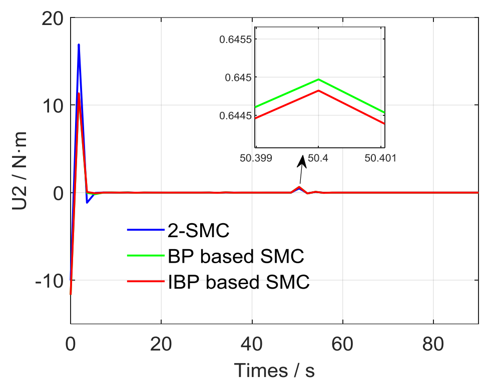

(b)

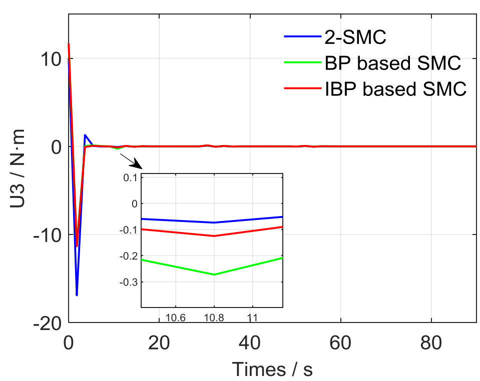

(c)

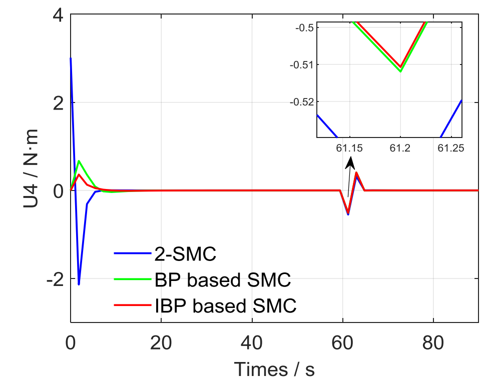

(d)

Fig.7. Control inputs

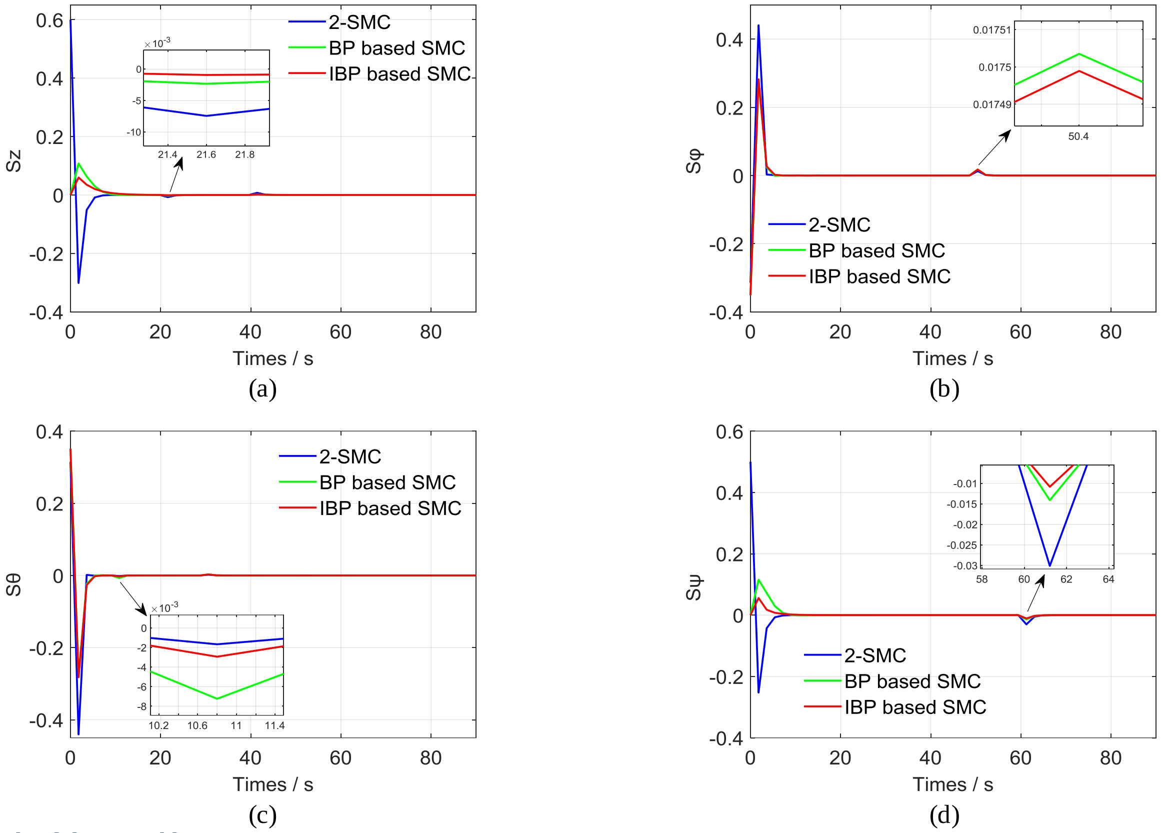

Fig.8. The sliding variables

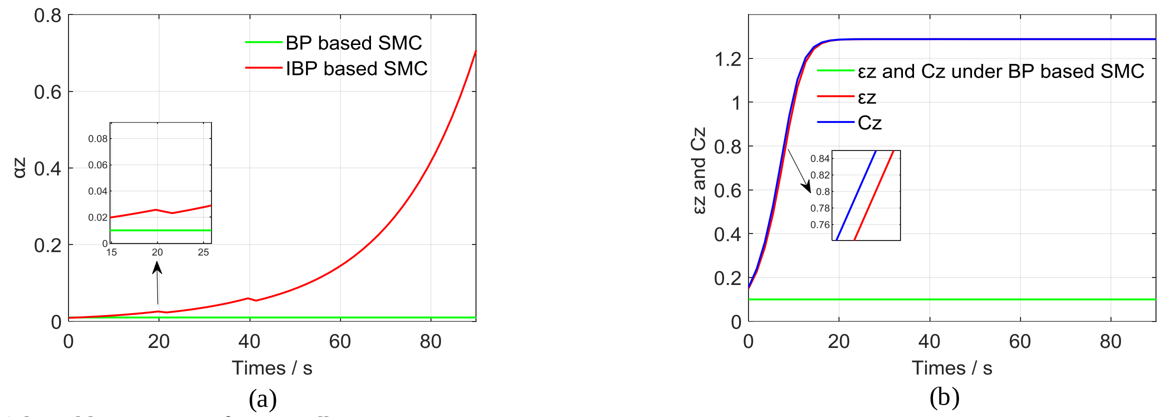

Fig.9. Adjustable parameters for controller U1

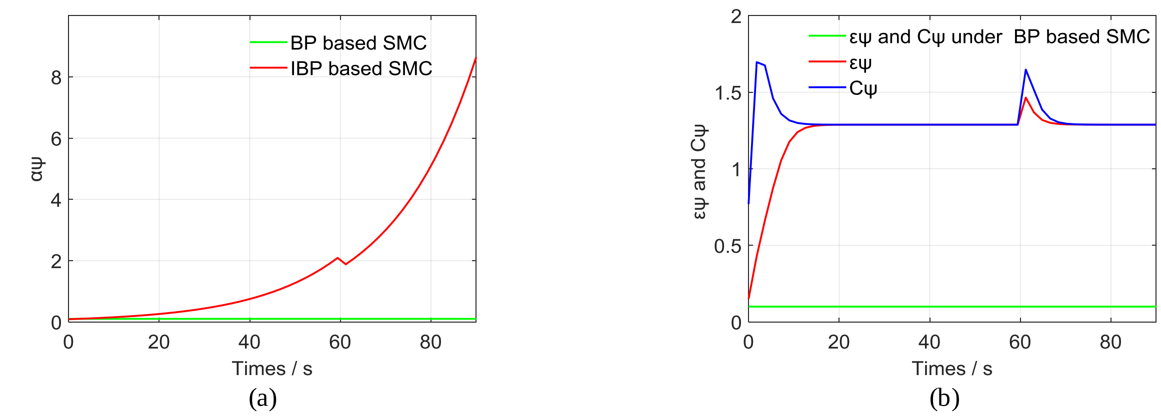

Fig.10. Adjustable parameters for controller U4

Fig. 7 shows a comparison of the four control inputs over time under the control of three methods. It can be seen from the figure (a), (b), (c), (d) that, compared with the other two methods, the control input under the proposed method has fewer chattering phenomena and its maximum overshoot is significantly smaller when chatter occurs, which ensures the stability of the control input.

Fig. 8 shows the results of the four designed sliding manifolds over time under the control of three methods. It can be seen from the figure (a), (b), (c), (d) that the designed sliding manifold gradually attenuates and converges to near the equilibrium point 0 within a finite time. However, compared with the other two methods, the chatter of the sliding manifold designed under the proposed method has a good suppression of chatter, and the maximum overshoot is also small.

Fig. 9 and 10 respectively show the results of the designed parameters of control input U_1 (9(a) & 9(b)) and U_4 (10(a) & 10(b)) changing over time. It can be found that under the proposed method, its parameters can be adjusted dynamically. Because of this, it produces a better control effects than the other two methods.

In conclusion, the proposed method can effectively track the desired position and attitude. Compared with 2-SMC and standard BP network, it can effectively suppress the chatter phenomenon during the whole tracking process, and also greatly reduce the maximum overshoot when the chatter phenomenon occurs, making the controller more stable and reliable.

6. CONCLUSIONS

The Improved BP network based sliding model tracking control for a quadrotor UAV proposed in this paper effectively realizes the accurate tracking of the position and attitude of the quadrotor UAV. In order to verify the effectiveness of the controller designed under the proposed method, a simulation comparison experiment was carried out through the Matlab/ Simulink simulation platform, and the main conclusions are as follows:

• The proposed method of first calculating the expected roll angle and expected pitch angle according to the desired state, and then designing the controller can make the parameter uncertainty of the quadrotor UAV be compensated more accurately, and prevent the occurrence of more chattering phenomenon with larger overshoot due to over-compensation, which is beneficial to ensure the stability of the tracking process.

•All state variables (position and attitude) can effectively converge to the expected state in a finite time, and can quickly recover to a stable state even in the case of continuous time-varying switching of control signals, which has good adaptability and universality.

•Compared with the 2-SMC and the standard BP network, the improved BP network can effectively suppress the chatter phenomenon, and greatly reduces the maximum overshoot.

•It effectively expands the application range of neural network algorithm.

ACKNOWLEDGEMENT

This work was partially supported by the National Natural Science Foundation of China under Grant No.62073334.

DATA AVAILABILITY

The data that support the findings of this study are included within the article.

CONFLICTS OF INTEREST

The authors declare that they have no conflicts of interest.

REFERENCES

Alejandro G-G, David B-A, Ivana C-G, et al. (2020). Control of an Unmanned Surface Vehicle based on adaptive dynamic programming and deep reinforcement learning. *Pro of the international conference on deep learning technologies*, 118-122.

ALVEAR O, CALAFATE C T, ZEMA N R, et al. (2018). A discretized approach to air pollution monitoring using UAV-based sensing. *Mobile Networks and Applications*, 23(6), 1693-1702.

A. Zulu, S. John. (2014). A review of control algorithms for autonomous quadrotors. *Open J. Appl. Sci*, 4, 547–556.

F.R. Lopez-Estrada, J.C. Ponsart, D. Theilliol, et al. (2016). LPV Model-Based Tracking Control and Robust Sensor Fault Diagnosis for a Quadrotor UAV. *Journal of Intelligent & Robotic Systems*, 84, 163-177.

G. Cao, E.M.-K. Lai, F. Alam. (2017). Gaussian Process Model Predictive Control of an Unmanned Quadrotor. *Journal of Intelligent & Robotic Systems*, 88, 147-162.

Hadi R. (2018). Adaptive neural network based sliding mode altitude control for a quadrotor UAV. *Journal of Central South University*, 25(11), 2654–2663.

Hadi R, Sima A. (2019). Neural network-based adaptive sliding mode control design for position and attitude control of a quadrotor UAV. *Aerospace Science and Technology*, 91, 12-17.

H. Casta, J.L. Gordillo. (2019). Spatial Modeling and Robust Flight Control Based on Adaptive Sliding Mode Approach for a Quadrotor MAV. *Journal of Intelligent & Robotic Systems*, 93, 101-111.

J. Moreno-Valenzuela, R. Pérez-Alcocer, M. (2019). Guerrero-Medina, et al. Nonlinear PID-Type Controller for Quadrotor Trajectory Tracking. *IEEE/ASME Trans. Mechatron*, 23(5), 2436-2447.

Kaifang W, Xiaoguang G, Zijian H and Gaofeng W. (2020). Robust Motion Control for UAV in Dynamic Uncertain Environments Using Deep Reinforcement Learning. *Remote Sens*, 12, 640.

Khebbache, H., Tadjine, M. (2013). Robust Fuzzy Backstepping Sliding Mode Controller For a Quadrotor Unmanned Aerial Vehicle. *Journal of Control Engineering and Applied Informatics*. 15(2):3–11.

Manyam S G, Rasmussen S, Casbeer D W, et al. (2017). Multi-UAV routing for persistent intelligence surveillance and reconnaissance missions. *Proc. of International Conference on Unmanned Aircraft Systems*, 573-580.

M. Faessler, D. Falanga, D. Scaramuzza. (2017). Thrust Mixing, Saturation, and Body-Rate Control for Accurate Aggressive Quadrotor Flight. *IEEE Robotics Automation Letters*, 2(2), 476-482.

M. Hassanalian, A. Abdelkefi. (2017). Classifications, applications, and design challenges of drones: a review. *Prog. Aerosp*, 99–131.

M. Labbadi, M. Cherkaoui. (2019). Robust adaptive backstepping fast terminal sliding model controller for uncertain quadrotor UAV. *Aerospace Science and Technology*, 93, 1-14.

O. Mofid, S. Mobayen. (2018). Adaptive sliding mode control for finite-time stability of quad-rotor UAVs with parametric uncertainties. *ISA Transactions*, 72, 1-14.

Petr S, Jaroslav K, Jan D. (2018). Using unmanned aerial system in military operations for autonomous reconnaissance. *Proc. of International Conference on Modelling and Simulation for Autonomous Systems*, 514-529.

R.C. Avram, X. Zhang, J. Muse. (2017). Quadrotor Actuator Fault Diagnosis and Accommodation Using Nonlinear Adaptive Estimators. *IEEE Trans. Control Systems Technology*, 25(6), 2219–2226.

WU B, HAN S, XIAO J, HU X, FAN J. (2016). Error compensation based on BP neural network for airborne laser ranging. *Optik-International Journal for Light and Electron Optics*, 127(8), 4083–4088.

XIONG J J, ZHANG G B. (2016). Global fast dynamic terminal sliding mode control for a quadrotor UAV. *ISA Transactions*, 66, 233-240.

Y. Yang, Y. Yan. (2016). Attitude regulation for unmanned quadrotors using adaptive fuzzy gain-scheduling sliding mode control. *Aerospace Science and Technology*, 54: 208-217.

Zheng E-H, Xiong J-J, Luo J-L. (2014). Second order sliding mode control for a quadrotor UAV. *ISA Transactions*, 53(4), 1350-1356.

Z. Jia, J. Yu, Y. Mei, et al. (2017). Integral backstepping sliding mode control for quadrotor helicopter under external uncertain disturbances. *Aerospace Science and Technology*, 68, 299-307.